

ROUGH-WALL HEAT TRANSFER AT MODERATE PRANDTL NUMBERS: TOWARDS RECONCILING THE DIVERSE MODEL PREDICTIONS

Kevin Zhong¹, Nicholas Hutchins¹, and Daniel Chung¹

1: Department of Mechanical Engineering, University of Melbourne, VIC 3010, Australia,
kevin.zhong@student.unimelb.edu.au

ABSTRACT

In the fully rough regime, a rough-wall heat transfer coefficient, e.g. the roughness Stanton number, takes the form $St_k \sim (k^+)^{-p} Pr^{-m}$, but proposed values for p and m vary, giving diverse predictions. Here, k^+ is the viscous-scaled roughness size and Pr is the Prandtl number. To help clarify this, we conduct direct numerical simulations of forced convection in a rough-wall channel for $Pr = 0.5, 1.0$, and 2.0 , sweeping from transitional to fully rough conditions by varying k^+ . Minimal channels are used, which resolve the roughness sublayer at affordable cost enabling an extensive parametric study. In predicting the mean heat transfer, we find that our data favours the so-called surface renewal phenomenology of Brutsaert (1975), which predicts $p = 1/4, m = 1/2$ over the Reynolds–Analogy-type phenomenologies, which predict $p = 1/2$ for the fully rough regime. For the transitionally rough regime, conventional understanding argues that turbulence retains a form similar to that of a smooth wall flow except for an offset (Luchini, 1996). We show in our low- k^+ data that these ideas, although originally describing momentum transfer, can also generalize well to turbulent heat transfer.

INTRODUCTION

In engineering and environmental applications, we often encounter wall-bounded turbulent flows involving the transport of passive scalars such as temperature or contaminants. The wall is seldom smooth in practice and is instead rough, causing drag and heat transfer enhancements. Heat transfer at a solid surface occurs through molecular conduction which depends on the thermal diffusivity of the fluid α and is accounted for through the molecular Prandtl number $Pr \equiv \nu/\alpha$ where ν is the kinematic viscosity. In turbulent heat transfer, the influence of a rough-wall can be represented through intercepts to the logarithmic temperature profile, Θ^+ (Chung *et al.*, 2021):

$$\Theta^+ \equiv \frac{\Theta}{\Theta_\tau} = \frac{1}{\kappa_\theta} \log[(z-d)^+] + A_\theta(Pr) - \Delta\Theta^+(k^+, Pr) \quad (1)$$

$$= \frac{1}{\kappa_\theta} \log[(z-d)/z_0] + St_k^{-1}(k^+, Pr) \quad (2)$$

$$= \frac{1}{\kappa_\theta} \log[(z-d)/k_s] + g(k^+, Pr) \quad (3)$$

where $\Theta(z-d)$ is the mean temperature relative to the wall which varies with wall-normal distance, z , and d represents a virtual-origin offset such that $z-d$ measures the wall-normal distance from the virtual origin plane (Chung *et al.*, 2021). Here, $\kappa_\theta \approx 0.46$ and $\Theta_\tau \equiv \langle q_w \rangle / (\rho c_p U_\tau)$ is the friction temperature with $\langle q_w \rangle$ being the global heat flux defined on the

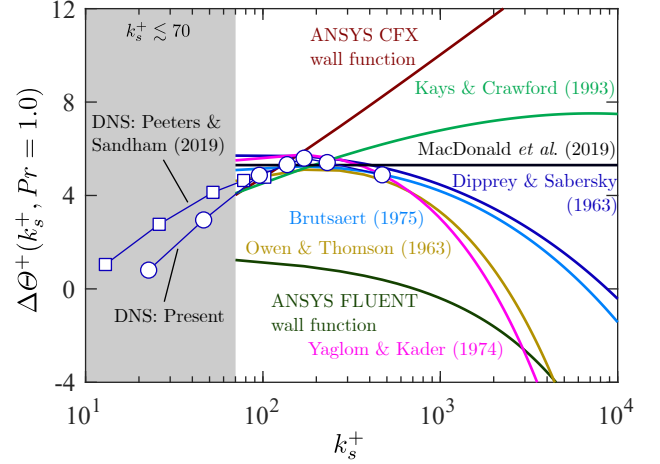


Figure 1. The disparate predictions by heat transfer models at $Pr = 1.0$ for heat-transfer augmentation $\Delta\Theta^+$ in the fully rough regime ($k_s^+ \gtrsim 70$). The models (solid lines) are tuned to fit the trends of the high- k_s^+ DNS (markers).

plan area, density ρ , specific heat capacity c_p and global friction velocity $U_\tau \equiv \sqrt{\tau_w/\rho}$ where τ_w is the wall shear stress. The $+$ superscripts denote normalizations on Θ_τ, U_τ , and ν e.g. $z^+ \equiv zU_\tau/\nu$. The formulation of (1) represents the effects of roughness through a heat transfer augmentation $\Delta\Theta^+(k^+, Pr)$ relative to the smooth-wall intercept A_θ , and depends on the roughness Reynolds number $k^+ \equiv kU_\tau/\nu$ where k is a representative roughness size. Equation (2) adopts the roughness Stanton number St_k based on z_0 coordinates (Kays & Crawford, 1993), where z_0 is defined by the logarithmic mean velocity profile $U^+ = (1/\kappa) \log[(z-d)/z_0]$ with $\kappa \approx 0.4$ (Brutsaert, 1982). Equation (3) uses the g -function defined on the equivalent sand-grain roughness k_s (Dipprey & Sabersky, 1963). Models for the fully rough regime usually have the form $St_k^{-1} \sim g \sim (k^+)^p Pr^m$, which have seen diverse proposals for the exponents $p = 0.20-0.50, m = 0.44-0.80$, both empirically and phenomenologically motivated (Chung *et al.*, 2021). The correct values to take for p and m remain ambiguous (Li *et al.*, 2020) and this difficulty is illustrated in figure 1 which shows fully rough models for $Pr = 1.0$. Each model has coefficients which can be tuned to fit the high- k_s^+ direct numerical simulation (DNS) data, making inspection of model trends alone insufficient in discerning the correct values to take for the exponents. Moreover, figure 1 presents data for only a single working fluid (i.e. fixed $Pr = 1.0$) and thus does not inform us as to how well the models generalize to arbitrary working fluids. Rather than compare model trends, a

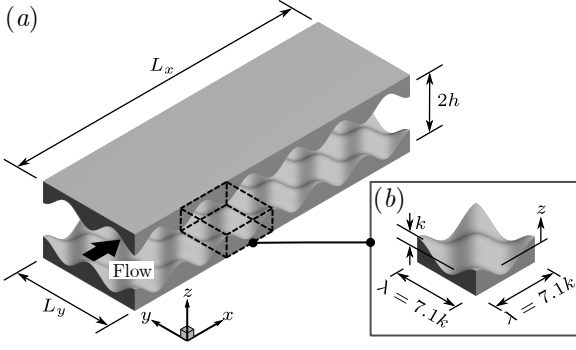


Figure 2. (a) Channel flow schematic (not to scale). The channel half-height h is measured from the sinusoid midplane. (b) The present 3D sinusoids have amplitude k and fixed wavelength $\lambda = 7.1k$.

more robust approach is instead, to test the physical assumptions which underpin these models against high-fidelity DNS data. The difficulty in this approach however, lies in the stringent computational cost associated with sweeping the (k^+, Pr) parameter space. Our present work will circumvent these difficulties through the use of minimal channels, which can accurately resolve the roughness sublayer at affordable cost and thereby measure the various log-intercepts in equations (1–3) (MacDonald *et al.*, 2019). With a comprehensive set of DNSs available, we scrutinise some of the phenomenologies describing fully rough heat transfer. These phenomenologies fall into two categories: the surface renewal phenomenology of Brutsaert (1975) which proposes $p = 1/4$, $m = 1/2$ and Reynolds-Analogy-type phenomenologies which propose $p = 1/2$ with $m = 2/3$ or $m = 3/4$ (Owen & Thomson, 1963).

In the transitionally rough regime, characterized by low-to-moderate values of k^+ , our conventional understanding of this regime is one where the near-wall turbulence retains a form similar to that of a smooth wall, except shifted by an offset (Luchini, 1996). We will show in our low- k^+ DNS that some of these concepts can generalize well to the case of turbulent heat transfer.

DIRECT NUMERICAL SIMULATIONS

We consider a channel flow as illustrated in figure 2(a) and denote (x, y, z) as the streamwise, spanwise, and wall-normal directions. We solve the incompressible Navier–Stokes equations and the passive-scalar equation for the fluid temperature, θ using a fourth-order finite-difference method. The flow is forced at a constant mass flux, while the temperature is driven through a streamwise-linearly-varying wall temperature gradient. The roughness is a 3D sinusoid with semi-amplitude k and wavelength $\lambda = 7.1k$ (figure 2b), defined by $z_w(x, y) = k \cos(2\pi x/\lambda) \cos(2\pi y/\lambda)$ and is mirrored on the top and bottom walls of the channel (figure 2). No-slip and zero fluid–wall temperature contrast ($\theta = 0$) conditions are imposed through an immersed-boundary method. Our study spans transitional cases at $k^+ \approx 5.5$ towards the fully rough regime at $k^+ \approx 111$ for Prandtl numbers, $Pr = 0.5, 1.0$, all documented in table 1. The friction Reynolds number varies from $Re_\tau \equiv hU_\tau/\nu = 395\text{--}2000$ and the blockage ratio is $h/k \geq 18$. Minimal channels are used, which truncate the domain lengths $L_x \times L_y$ whilst resolving the roughness sublayer and for all cases remain below the unphysical flow-region $z = z_c \approx 0.4L_y$ (MacDonald *et al.*, 2019), thus enabling an extensive set of 21 total rough-wall DNSs. Prescriptions for the domain

sizes follow from MacDonald *et al.* (2017). Namely, $L_x \geq \max(3L_y, 1000\nu/U_\tau, \lambda)$ and $L_y \geq \max(100\nu/U_\tau, k/0.4, 2\lambda)$. The latter condition of $L_y \geq 2\lambda$ has been modified from MacDonald *et al.* (2017) so as to ensure the unphysical region, z_c , lies above the roughness sublayer, which is approximately $z_r \approx \lambda/2$ for our present sinusoids (Chan *et al.*, 2018). Further smooth-wall minimal channel DNSs were also conducted at matched Re_τ and domain sizes with those outlined in table 1 to obtain domain-size-independent measures of the log-intercepts in (1–3). For these log-intercept measurements to be robust, we must measure from the virtual origin by accounting for a shift, d , (Chung *et al.*, 2021). Presently, we have defined d to be the upwards displacement from the sinusoid midplane. For low- k^+ , d can be understood as a displacement of smooth-wall turbulence, which can be obtained by shifting the Reynolds shear stress profiles to collapse with a smooth wall profile (García-Mayoral *et al.*, 2019). This approach has been adopted for our $k^+ = [5.5, 11, 22]$ cases and yielded $d/k = [0.18, 0.15, 0.36]$. At higher- k^+ , this method may no longer hold as the near-wall turbulent structure differs greatly from that of a smooth wall (Jiménez, 2004). Our approach here has been to perform an ad-hoc tuning of d to give a best-fit to the logarithmic slopes, $\kappa \approx 0.4$, $\kappa_\theta \approx 0.46$ which yielded the empirical fit $d/k = -(k^+/365)^2 + (k^+/213) + 0.27$ and is fitted to our $k^+ = [33, 40, 56, 111]$ cases. Measures for e.g. $\Delta\Theta^+$ are then taken to be the difference between the smooth wall and rough wall temperature profiles evaluated at the minimal channel critical height: $\Delta\Theta^+ \equiv \Theta_{\text{smooth}}^+(z_c^+) - \Theta_{\text{rough}}^+(z_c^+)$ and are provided in table 1. We also measured the roughness functions at various heights above the roughness sublayer thickness, $z_r \approx \lambda/2$ and below z_c , which resulted in negligible variations for $\Delta\Theta^+$ no greater than 0.3.

THE FULLY ROUGH REGIME

In figure 3(a), we present measurements of the g -function in (3) against k_s^+ coordinates where $k_s^+ = 2.7k^+$ for our present 3D sinusoids, obtained by collapsing fully rough drag measurements with the Nikuradse curve: $\Delta U^+ = (1/0.4) \log(k_s^+) - 3.5$ (not shown) (Nikuradse, 1933). The data is shown alongside the $Pr = 0.7$ DNS of MacDonald *et al.* (2019) for identical 3D sinusoids (note that the present data have a different k_s/k due to different virtual origin treatments), and the $Pr = 1.2\text{--}5.9$ data of Dipprey & Sabersky (1963) for close-packed granular roughness. In the fully rough regime, both roughness types favour $p = 1/4$ more closely than $p = 1/2$ in $g \sim (k^+)^p \sim (k_s^+)^p$. The empirical fits for $g \sim (k_s^+)^p Pr^m$ in figure 3(b) yield $p = 0.20$, $m = 0.40$, similar to values of Dipprey & Sabersky (1963) and are close to the analytical $p = 1/4$, $m = 1/2$ proposals of Brutsaert (1975). We observe in figure 3(c) that plotting $St_k^{-1} \sim g$ against $(z_0^+)^{1/4} Pr^{1/2}$ is able to collapse the fully rough data onto a single asymptote. Here, a switch is made from k_s to z_0 where $k_s/z_0 \approx 30$ in the fully rough regime, and $z_0^+ \approx 0.135$ for a smooth wall. Figure 3(c) then provides an overall view for heat transfer, from smooth to fully rough under a variety of working fluids. In figure 3(d), we show the roughness function $\Delta\Theta^+$, which appears to plateau at $k_s^+ \approx 100$ before beginning a gradual decrease. It is unclear whether this continual decrease of $\Delta\Theta^+$ towards a negative value will eventually occur, as this would imply a reduction in heat transfer relative to a smooth wall, which stands in contrast to conventional understanding of rough-wall heat transfer (Kays & Crawford, 1993). The observed $\Delta\Theta^+$ behaviour is also in contrast to drag which increases with k_s^+ according to the fully rough asymp-

Re_τ	Pr	h/k	k^+	L_x^+	L_y^+	N_x	N_y	N_z	Δx^+	Δy^+	Δz_b^+	Δz_t^+	ΔU^+	$\Delta \Theta^+$
395	0.5	72	5.5	1091	156	768	128	420	1.42	1.22	0.26	5.55	1.5	0.3
395	1.0	72	5.5	1091	156	768	128	420	1.42	1.22	0.26	5.55	1.5	0.8
395	0.5	72	5.5	1091	156	768	128	560	1.42	1.22	0.21	3.89	1.5	1.9
395	0.5	36	11	1013	156	384	64	520	2.64	2.43	0.26	5.45	4.1	1.2
395	1.0	36	11	1013	156	384	64	520	2.64	2.43	0.26	5.45	4.1	2.9
395	1.0	36	11	1013	156	384	64	640	2.64	2.43	0.23	3.96	4.0	6.3
395	0.5	18	22	1091	312	192	64	660	5.68	4.87	0.28	5.54	6.7	2.0
395	1.0	18	22	1091	312	192	64	660	5.68	4.87	0.28	5.54	6.8	4.7
395	2.0	18	22	1091	312	192	64	660	4.26	2.43	0.24	3.76	6.9	8.9
590	0.5	18	33	1396	465	324	108	920	4.31	4.31	0.29	6.34	8.0	2.6
590	1.0	18	33	1396	465	324	108	920	4.31	4.31	0.29	6.34	8.0	5.0
590	2.0	18	33	1396	465	456	152	1120	3.06	3.06	0.25	5.00	8.0	9.0
720	0.5	18	40	1704	568	384	128	1180	4.44	4.44	0.29	5.59	8.4	2.7
720	1.0	18	40	1704	568	384	128	1180	4.44	4.44	0.29	5.59	8.6	5.2
720	2.0	18	40	1704	568	468	156	1360	3.64	3.64	0.25	5.12	8.5	9.1
1000	0.5	18	56	2367	789	576	192	1560	4.11	4.11	0.29	6.58	9.3	2.8
1000	1.0	18	56	2367	789	576	192	1560	4.11	4.11	0.29	6.58	9.6	5.2
1000	2.0	18	56	2367	789	512	384	1860	4.62	2.05	0.24	5.39	8.7	8.7
2000	0.5	18	111	4733	1578	1080	360	2700	4.38	4.38	0.29	10.6	10.9	2.8
2000	1.0	18	111	4733	1578	1080	360	2700	4.38	4.38	0.29	10.6	10.8	4.7
2000	2.0	18	111	4733	1578	1024	768	3200	4.62	2.05	0.25	8.58	11.0	7.1

Table 1. Table of simulations for the present study. N_x , N_y , and N_z are the number of grid points in the streamwise, spanwise, and wall-normal directions, with uniform grid spacings Δx^+ and Δy^+ , while the wall-normal grid spacing is given by the (constant) grid spacing below the roughness crests Δz_b^+ and the spacing at the channel centreline Δz_t^+ .

tote: $\Delta U^+ = (1/0.4) \log(k_x^+) - 3.5$, owing to the dominance of pressure drag, a phenomena which has no analogue in heat transfer (Owen & Thomson, 1963). The velocity-temperature dissimilarity in the fully rough regime is visualized in figure 4, which shows that the surface area is covered predominantly by recirculated ($u^+ < 0$) flow which mixes the temperature, with the well-mixedness improving for higher Pr . The significant temperature variations are confined primarily to the local conductive sublayer thickness, which conforms to the roughness topography shape as noted by MacDonald *et al.* (2019) and becomes thinner with increasing Pr . The conductive sublayer is observed to be thinnest in windward faces, where fluid impinges on the rough surface creating sharper velocity and temperature gradients and thereby, regions of higher local heat-transfer (Peeters & Sandham, 2019). As noted in Leonardi *et al.* (2015); Foroughi *et al.* (2018), at leeward faces where low-speed, stagnant fluid resides, a well-mixed region of temperature with small temperature gradients tends to form, thereby producing the thicker conductive sublayers observed in these regions (figure 4d–f).

THE TRANSITIONALLY ROUGH REGIME

In the fully rough regime, we observed in figure 4 that the conductive sublayer appears as a thin layer relative to the roughness size and conforms to the roughness topography. In the transitionally rough regime however, where k^+ is low-to-moderate, the roughness size k can be comparable to the conductive sublayer thickness such that the conductive sublayer no longer conforms to the roughness topography like in the fully rough regime. Instead, as illustrated in figure 5, the near-wall flow of low- k^+ regimes retain a quiescent state akin to that observed in the viscous–conductive regions of a smooth wall flow. Here, we follow the idea of Luchini (1996), arguing that the heat transfer augmentation, $\Delta \Theta^+$, in these regimes can be expressed through a displacement perceived by the mean temperature, ℓ_Θ and a displacement of the turbulence d , which, when accounted for, can collapse the mean temperature with a smooth wall profile. The full procedure is illustrated in figure 6. Here, the displacement d , as elaborated in García-Mayoral *et al.* (2019) can be determined by collapsing the Reynolds shear stress profiles with smooth wall profiles and here, we have assumed that the displacement of the turbulence perceived by both the momentum

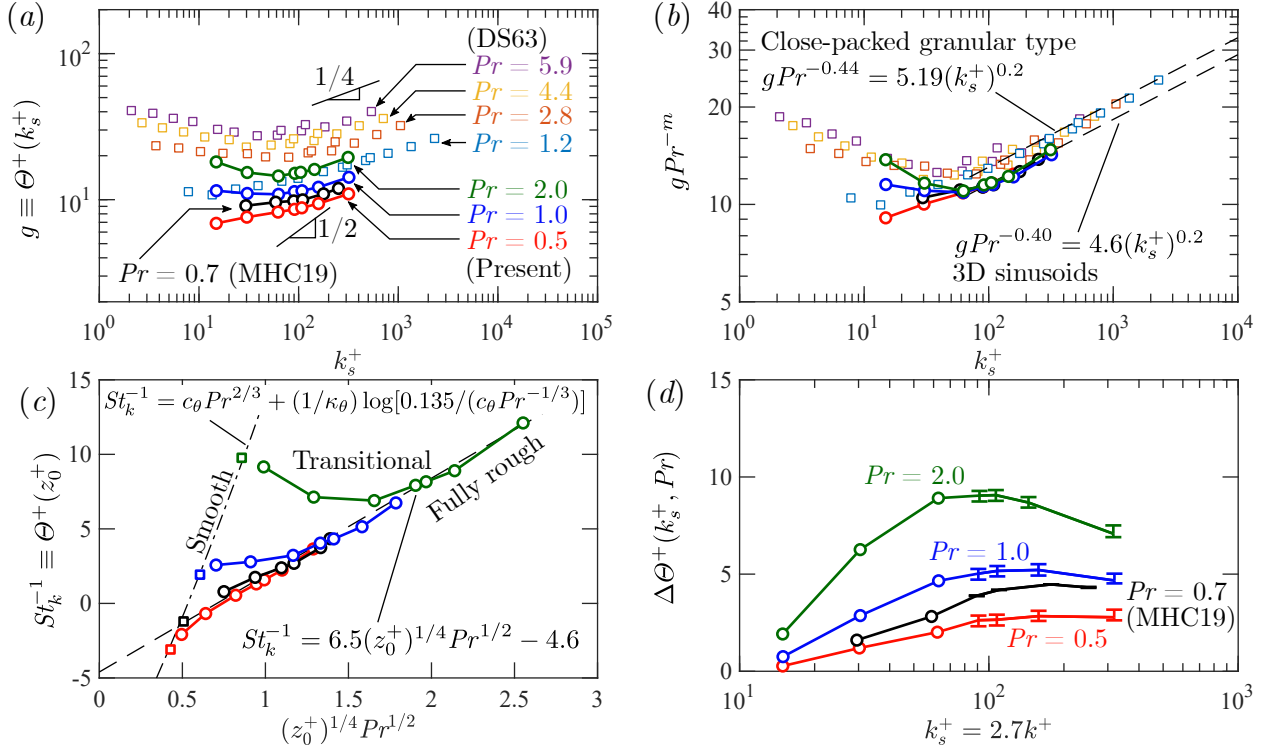


Figure 3. Log-intercept measurements in equations (1–3). (a,b) Log-intercept $g(k_s^+, Pr)$ for present 3D sinusoids compared against the $Pr = 1.2$ – 5.9 close-packed granular type roughness of Dipprey & Sabersky (1963), with empirical fits given in (b). Also included are the $Pr = 0.7$ DNS of MacDonald *et al.* (2019) for identical 3D sinusoids. (c) The roughness Stanton number St_k on z_0 coordinates, presenting the behaviours of heat transfer from smooth ($c_\theta \approx 11.3$) to fully rough, where the $St_k^{-1} \sim (z_0^+)^{1/4} Pr^{1/2}$ scaling of Brutsaert (1975) predicts the fully rough data well. The square markers are smooth-wall DNS. (d) Heat transfer augmentation $\Delta\Theta^+$ for the present 3D sinusoids DNS. The error bars for high- k_s^+ correspond virtual origin measurements at the sinusoid midplane and crests.

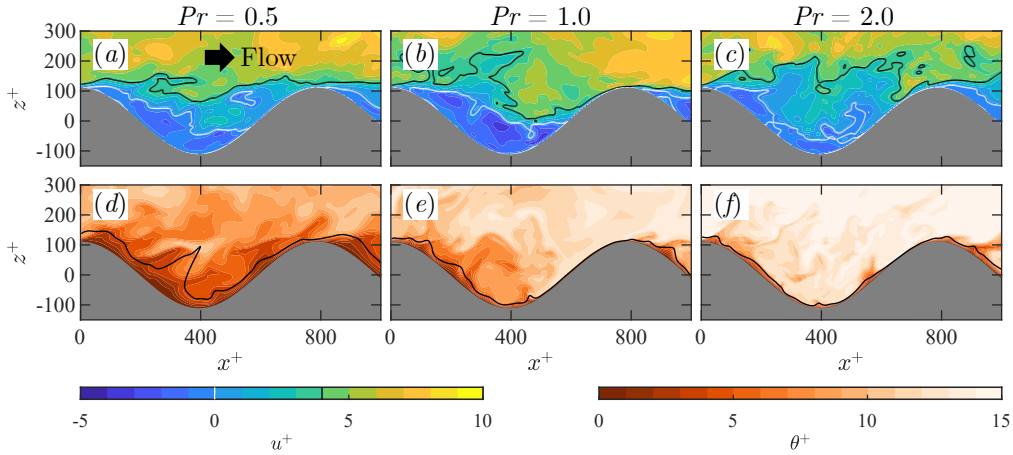


Figure 4. (a–c) Instantaneous streamwise velocity contours at $k^+ \approx 111$ with contour levels at $u^+ = 0, 4$ (white, black) to highlight stagnant fluid regions and the slip velocity across the crests respectively. (d–f) The corresponding temperature fields for $Pr = 0.5$ – 2.0 , where black lines trace instantaneous measurements of the local conductive sublayer, which tracks the regions where the local temperature varies linearly.

and temperature fields are the same (i.e. $d_\theta \approx d$). The mean displacement location $z = \ell_\theta$ is measured relative to the sinusoid midplane and is defined as the distance where the mean temperature reaches its wall value ($\Theta^+ = 0$) based on an extrapolation of the mean temperature profile above the roughness and within the conductive sublayer such that the temperature gradient matches that of a smooth wall conductive sub-

layer: $d\Theta^+/dz^+ = Pr$ (figure 6b) (Kader, 1981). The framework of Luchini (1996) proposes that measuring from the turbulence origin $(z-d)^+$ is what enables the rough-wall profiles to now follow the shape of a smooth-wall profile that is situated at the turbulence origin, only offset by an amount $\Theta_{\text{smooth}}^+ - \Theta_{\text{rough}}^+ = \Delta\Theta^+$ which is assumed to be a constant that propagates into the log region. As illustrated in figure 6(c), the

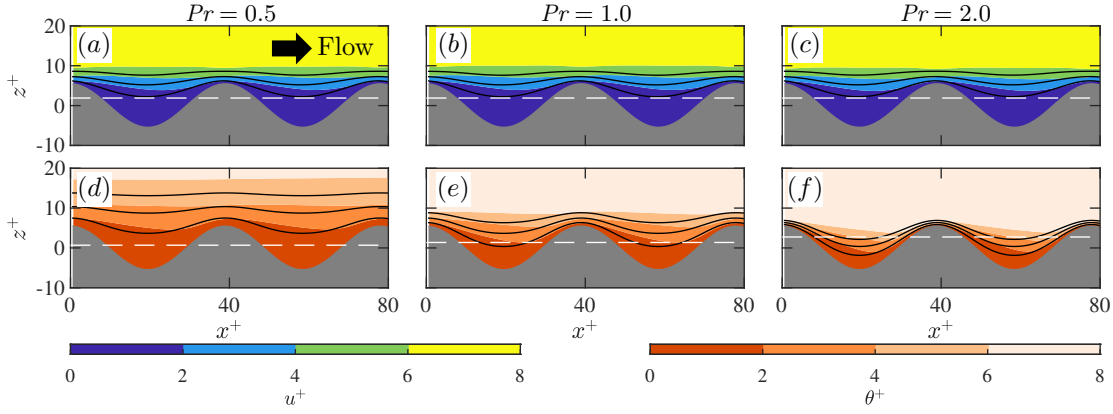


Figure 5. (a–c) Time-averaged velocity and (d–f) temperature fields at $k^+ \approx 5.5$. The solid black lines overlay Stokes flow calculations, which are converted to an equivalent wall-unit scaling via $u_{\text{Stokes}}^+ = [u_{\text{Stokes}} / (k_{\text{Stokes}} dU/dz|_{\text{Stokes}})] k^+$, $\theta_{\text{Stokes}}^+ = [\theta_{\text{Stokes}} / (k_{\text{Stokes}} d\theta/dz|_{\text{Stokes}})] Pr k^+$. The Stokes subscripts denote values from the Stokes flow calculations and the mean profile gradients dU/dz , $d\theta/dz$ are measured in the homogeneous region above the roughness. These transformations allow for matching with the viscous–conductive gradients in the DNS, i.e., $dU_{\text{Stokes}}^+ / dz_{\text{Stokes}}^+ = 1$, $d\theta_{\text{Stokes}}^+ / dz_{\text{Stokes}}^+ = Pr$ with $z_{\text{Stokes}}^+ = (z/k_{\text{Stokes}}) k^+$. The white lines locate the mean displacement origins of Stokes flow for (a–c) velocity, $\ell_u^+ = (\ell_u/k) k^+$ and (d–f) temperature, $Pr \ell_\theta^+ = (\ell_\theta/k) Pr k^+$.

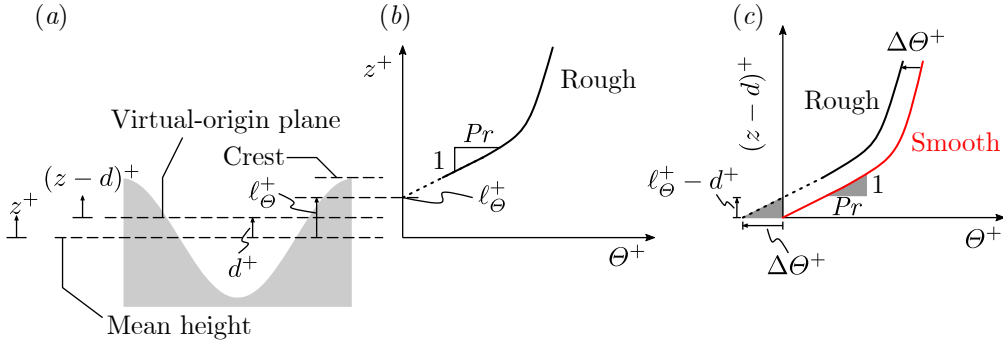


Figure 6. Schematic illustration of the virtual-origin framework in low- k^+ flows. (a) Reference locations of the present terminology. (b) An example rough-wall profile measured from the roughness mean height, z^+ , from which the mean temperature slip length ℓ_θ^+ is measured. (c) The virtual-origin shift being applied, now demonstrating the prediction $\Delta\theta^+ = Pr(\ell_\theta^+ - d^+)$, which results from the mean gradient constraint $d\theta^+/dz^+ = Pr$ (compare gray triangles).

new location of the mean temperature origin is now $(\ell_\theta - d)^+$ when measuring from $(z - d)^+$ and thus, with both smooth and rough walls having matched gradients, $d\theta^+/dz^+ = Pr$, predicts $\Delta\theta^+ / (\ell_\theta^+ - d^+) = Pr \iff \Delta\theta^+ = Pr(\ell_\theta^+ - d^+)$.

In figure 7, we demonstrate these shifts taking our lowest $k^+ \approx 5.5$ as an example case. Shown first in figure 7(a) are the mean temperature profiles measured from the mean roughness height, z^+ , which evidently show a discrepancy between the rough and smooth wall profiles. However, now measuring from the virtual-origin plane, $(z - d)^+$ and accounting for the temperature offset $\Delta\theta^+ = Pr(\ell_\theta - d)^+$, the collapse with the smooth wall profiles improve (figure 7b). The collapse is best for lower values of Pr , where the roughness elements have not significantly altered the conductive sublayer (figure 5). The analogous approach for velocity adopting the mean velocity displacement, ℓ_u^+ and the same turbulence displacement d^+ which yields the drag estimate $\Delta U^+ = (\ell_u^+ - d^+)$ (García-Mayoral *et al.*, 2019) is also shown in figure 7. Here, ℓ_u^+ is the mean velocity analogue to ℓ_θ^+ and the viscous sublayer velocity gradient instead follows $dU^+/dz^+ = 1$. For $k^+ \approx 5.5$, we find that $\ell_u/\ell_\theta \approx 1.5$, independent of Pr . This value is similar to the one we obtained from a Stokes flow calculation for our present roughness, $\ell_u/\ell_\theta \approx 1.4$ where the lower-case u and θ subscripts denote calculations of the same slip lengths ℓ_u , ℓ_θ

except from a Stokes flow. The mismatch $\ell_\theta \neq \ell_u$ implies drag and heat transfer augmentation caused by roughness differ even in the Stokes-flow-limit. The difference can be ascribed to the presence of pressure drag in the momentum field and its absence in the temperature field which can be inferred from the governing equations: $-\nabla p + \nabla^2 \mathbf{u} = 0$, $\nabla^2 \theta = 0$ where p is the pressure. Presently, we find $\ell_u/\ell_\theta \approx 1.2$, $\ell_\theta/\ell_\theta \approx 1.1$, and $d/\ell_v \approx 0.51$ (ℓ_v is the spanwise slip length, equal to ℓ_u for our present roughness). The theory of Luchini (1996) predicts that these ratios should approach unity provided we are operating in a viscous–conductive regime where $k^+ \rightarrow 0$. The non-unity values of these ratios indicate that our present $k^+ \approx 5.5$ is already too large to apply Stokes-flow predictions and can be observed visually in figure 5 by the mismatch of the Stokes flow calculations (solid black lines) and the $k^+ \approx 5.5$ DNS (coloured contours). The mismatch manifests as an upward shift relative to Stokes flow, suggesting that the advection introduced in the mean flow tends to be diverted away from the wall. This observation appears to be consistent with our measured $\ell_u/\ell_\theta > 1$, $\ell_\theta/\ell_\theta > 1$. That is, the mean flow origin is situated higher than the one predicted by Stokes flow. Despite the mismatch, our results in figure 7 suggest that a slip-length-type approach (Luchini, 1996) can still provide a valid avenue for modelling transitionally-rough heat transfer.

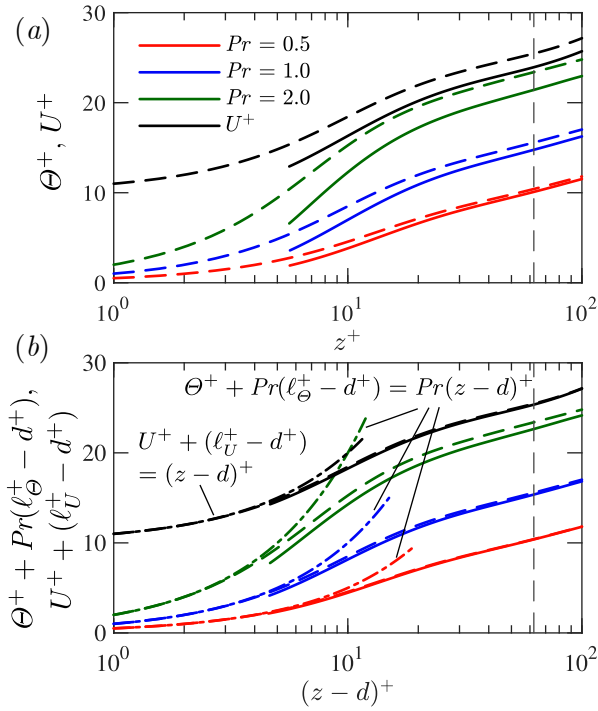


Figure 7. (a) Mean temperature (coloured) and velocity (black) profiles. Solid lines show profiles for the rough-wall ($k^+ = 5.5$) above the roughness crests ($z^+ > 5.5$). The velocity profiles are staggered by 10 on the y-axis for clarity. The dashed lines are smooth wall profiles at matched Pr and the vertical dashed line demarcates the physical region $z_c^+ = 0.4L_y^+$ of minimal channels. (b) The temperature profiles are shifted upwards by $Pr(\ell_\Theta^+ - d^+)$ and the velocity by $(\ell_U^+ - d^+)$ so that measuring from the virtual origin $(z - d)^+$ improves collapse with the smooth wall profiles ($d^+ = \ell_U^+ = \ell_\Theta^+ = 0$).

CONCLUSIONS

We have conducted a set of rough-wall DNSs, systematically varying both the Prandtl number and roughness Reynolds number k^+ from the transitional to fully rough regime. Our work addresses the ongoing ambiguity concerning fully rough heat transfer predictions, which typically have the form of a scaling for a roughness heat transfer coefficient: $St_k \sim (k^+)^{-p} Pr^{-m}$, the exponents p and m being topics of contention (Li *et al.*, 2017, 2020). We find that our data favours the model of Brutsaert (1975), which proposes $p = 1/4$, $m = 1/2$.

At lower- k^+ transitional regimes, the near-wall flow retains smooth wall characteristics, but shifted by an offset. Accounting for these shifts allows for the collapse of low- k^+ temperature profiles with smooth walls and implies a possible avenue for modelling transitionally-rough heat transfer.

ACKNOWLEDGEMENTS

We acknowledge the support of the Australian Research Council Discovery Project DP200100969. This research was supported by the Sustaining and strengthening merit-based access to National Computational Infrastructure (NCI) LIEF Grant (LE190100021) and facilitated by The University of Melbourne. We also acknowledge the assistance and resources from the National Computational Infrastructure (NCI Australia), an NCRIS enabled capability supported by the Australian Government and the resources provided by the

Pawsey Supercomputing Centre with funding from the Australian Government and the Government of Western Australia. We would also like to thank Prof. Detlef Lohse for providing feedback in this project and Mr. Jeremy Wong for helpful discussions concerning virtual-origin shifts.

REFERENCES

- ANSYS Inc. 2011 *ANSYS CFX-Solver Theory Guide*.
ANSYS Inc. 2013 *ANSYS Fluent Theory Guide*.
Brutsaert, W. 1975 A theory for local evaporation (or heat transfer) from rough and smooth surfaces at ground level. *Water Resour. Res.* **11** (4), 543–550.
Brutsaert, W. 1982 *Evaporation into the atmosphere: theory, history and applications*, , vol. 1. Springer Science & Business Media.
Chan, L., MacDonald, M., Chung, D., Hutchins, N. & Ooi, A. 2018 Secondary motion in turbulent pipe flow with three-dimensional roughness. *J. Fluid Mech.* **854**, 5–33.
Chung, D., Hutchins, N., Schultz, M. P. & Flack, K. A. 2021 Predicting the drag of rough surfaces. *Annu. Rev. Fluid Mech.* **53**, 439–471.
Dipprey, D. F. & Sabersky, R. H. 1963 Heat and momentum transfer in smooth and rough tubes at various Prandtl numbers. *Int. J. Heat Mass Transf.* **6** (5), 329–353.
Forooghi, P., Stripf, M. & Frohnepfel, B. 2018 A systematic study of turbulent heat transfer over rough walls. *Int. J. Heat Mass Transf.* **127**, 1157–1168.
García-Mayoral, R., de Segura, G. Gómez & Fairhall, C. T. 2019 The control of near-wall turbulence through surface texturing. *Fluid Dyn. Res.* **51** (1), 011410.
Jiménez, J. 2004 Turbulent flows over rough walls. *Annu. Rev. Fluid Mech.* **36**, 173–196.
Kader, B. A. 1981 Temperature and concentration profiles in fully turbulent boundary layers. *Int. J. Heat Mass Transf.* **24** (9), 1541–1544.
Kays, W. M. & Crawford, M. E. 1993 *Convective heat and mass transfer*, 3rd edn. McGraw-Hill.
Leonardi, S., Orlandi, P., Djenidi, L. & Antonia, R. A. 2015 Heat transfer in a turbulent channel flow with square bars or circular rods on one wall. *J. Fluid Mech.* **776**, 512–530.
Li, D., Rigden, A., Salvucci, G. & Liu, H. 2017 Reconciling the Reynolds number dependence of scalar roughness length and laminar resistance. *Geophys. Res. Lett.* **44** (7), 3193–3200.
Li, Q., Bou-Zeid, E., Grimmond, S., Zilitinkevich, S. & Katul, G. 2020 Revisiting the relation between momentum and scalar roughness lengths of urban surfaces. *Q. J. R. Meteorol. Soc.* .
Luchini, P. 1996 Reducing the turbulent skin friction. In *Computational Methods in Applied Sciences 1996, Proc. 3rd ECCOMAS CFD Conference*, pp. 465–470. Wiley.
MacDonald, M., Chung, D., Hutchins, N., Chan, L., Ooi, A. & García-Mayoral, R. 2017 The minimal-span channel for rough-wall turbulent flows. *J. Fluid Mech.* **816**, 5–42.
MacDonald, M., Hutchins, N. & Chung, D. 2019 Roughness effects in turbulent forced convection. *J. Fluid Mech.* **861**, 138–162.
Nikuradse, J. 1933 Laws of flow in rough pipes. English translation published 1950. *Tech. Rep.* 1292. NACA Tech. Mem.
Owen, P. R. & Thomson, W. R. 1963 Heat transfer across rough surfaces. *J. Fluid Mech.* **15** (3), 321–334.
Peeters, J. W. R. & Sandham, N. D. 2019 Turbulent heat transfer in channels with irregular roughness. *Int. J. Heat Mass Transf.* **138**, 454–467.